Baghdad Science Journal

Volume 22 | Issue 7 Article 2

7-16-2025

Adsorption of Pb(II), Cu(II), and Ni(II) by a New Magnetic Schiff Base Resin: Synthesis, Characterization, and Thermal Study

Iman Saad Ali
General Directorate of Basra Education, Basra, Iraq, imansaad086@gmail.com

How to Cite this Article
Ali, Iman Saad (2025) "Adsorption of Pb(II), Cu(II), and Ni(II) by a New Magnetic Schiff Base Resin: Synthesis, Characterization, and Thermal Study," *Baghdad Science Journal*: Vol. 22: Iss. 7, Article 2.
DOI: https://doi.org/10.21123/2411-7986.4982

BAGHDAD SCIENCE JOURNAL 2025;22(7):2144–2157

RESEARCH ARTICLE

Adsorption of Pb(II), Cu(II), and Ni(II) by a New Magnetic Schiff Base Resin: Synthesis, Characterization, and Thermal Study

Iman Saad Ali

General Directorate of Basra Education, Basra, Iraq

ABSTRACT

This study dealt with the preparation and analytical study of a type of chelating resin. This type of resin was distinguished by containing a ligand of the type of aromatic Schiff bases (5A-T) by reacting the aromatic amine (5-aminoisopthalic acid) with terephthaldehyde. The prepared Schiff base was identified using infrared FT-IR, ^{1}H-NMR, ^{13}C-NMR, and precise element analysis technology. The prepared Schiff bases were converted into azomethine-amide resin P5A-T by reacting the ligand (5A-T) with the diamines (4, 4-oxydianiline). The prepared resin was characterized using infrared spectroscopy.

The study also included the preparation of magnetic zinc iron oxide ($ZnFe_2O_4$) by covalent deposition method and its inoculation with the prepared resin P5A-T. $ZnFe_2O_4$ and the composite resin were diagnosed using several techniques, including scanning electron microscopy (FE-SEM), the particle size is (22 nm) for zinc iron oxide and (36 nm) for the composite magnetic resin. In addition, X-ray diffraction (XRD) technology was used in the diagnosis process, and the results confirmed the validity of the prepared composition. In addition, the magnetic properties of $ZnFe_2O_4$ and the prepared resin were studied and the composite resin showed superior magnetic behavior. The Malven Zetasizer device was used to measure the zeta potential. The last part included a study of the analytical efficiency in the adsorption of some heavy element ions (Ni^{+2}, Pb^{+2}, Cu^{+2}) using the batch method. The loading capacity of the prepared resins was studied under various conditions such as acid function and treatment time. The order of selectivity was Pb(II) > Cu(II) > Ni(II).

Keywords: Adsorbent, Chelating resin, Magnetic, Nanoparticles, Polyazomethine

Introduction

Growing industrialization has led to serious environmental issues. As result environmental problems are becoming more prevalent in many nations, particularly water contamination brought on by heavy metal ions. Cd (II) and Pb (II) are two heavy metals with high toxicity that can cause major harm to animals and humans throughout the food chain. According to a study by the United States Environmental Protection Agency, lead and cadmium can both cause lung cancer, hypertension, immune system disorders, and diseases of the reproductive and reproductive systems in children. Thus, it's crucial to eliminate heavy metal ions from water due to their high toxicity and lack of biodegradability.[1] Heavy metal ion contamination of the environment has received significant attention in recent years. Some of the frequently employed techniques for removing metal ions from effluents include filtering, chemical precipitation, chemical coagulation, flocculation, ion exchange, reverse osmosis, membrane technology, and solvent extraction.

These techniques, however, are constrained by their high operational costs and/or potential for ineffective removal of some harmful metal ions,

Received 28 October 2023; revised 29 March 2024; accepted 1 April 2024.
Available online 16 July 2025

E-mail address: imansaad086@gmail.com (I. S. Ali).

https://doi.org/10.21123/2411-7986.4982

particularly at trace level concentrations.[2] Researchers have recently become interested in polymer-based nanocomposites among the many other types of adsorbents that already exist due to the high potential they exhibit. PNCs are a brand-new category of hybrid materials that are typically created by mixing organic polymers with inorganic Nano fillers. The advantages of inorganic nano fillers, such as rigidity and temperature stability are combined with the special features of polymers, such as flexibility, ductility, and process ability. It's interesting to note that even at very low concentrations; nano fillers can change the macroscopic characteristics of polymers.[3] PNCs often have a large surface area, making them a suitable option for adsorption research because they have a considerable effect over this feature.[4] In aqueous solutions, this new adsorbent may form complexes with nearly all monovalent and divalent heavy metals, including Cu^{2+}, Pb^{2+}, Cd^{2+}, Hg^{2+}, $Zn^{2+,}$ Ag^{+}, and Ni^{2+}. Unfortunately, the TMT15 adsorbents are typically utilized as powders, making it challenging to remove them from suspension.[5] Consequently, nanoparticles-supported chelating resin technology has been used in nanoparticles adsorption approaches due to its special qualities that enable it to swiftly and effectively remove practically all types of contaminants. Nanoparticle adsorbent technology has been applied in nanoparticle adsorption technologies because of its unique properties that allow it to remove almost all types of contaminants very quickly and efficiently. Nano magnetic adsorbents are used as support materials and can be easily separated from the reaction media by means of a magnetic field. A magnetic field is employed to easily separate the reaction medium from the nano-magnetic adsorbents, which are used as support materials. Additionally, it has various benefits in that it does not generate secondary waste and that the materials employed are easily recyclable and adaptable to a variety of industrial applications. Additionally, metallic species can be eliminated from water, food, or medicine using magnetic adsorbents.[6] The purpose of this study is to create new polyamide with ladder-type structures containing azomethine groups. Because of their improved chemical stability due to their ladder-like structure, polyamides are a good choice for removing heavy metal ions from industrial effluents.

Materials and methods

The technique involved dissolving (2.1 g, 0.01 mol) of amine (5-aminoisophthalic acid) in (40 ml) of methanol and adding (2.6 g, 0.02 mol) of aldehyde (terephthaldehyde) in (10 ml) of methanol. The reaction was successful after retrograde escalation for 4 hours, followed by TLC, filtering, cooling, and the formation of a white precipitate. The white precipitate was then filtered, dried in a drying oven, and recrystallized with chloroform, with a melting point of 301 to 302°C.

Fig. 1 depicts synthetic route of Schiff base compound [5A-T]. The infrared spectrum (FT-IR), the nuclear magnetic resonance spectrum (^{1}H-NMR) spectrum (^{13}C-NMR), the exact elemental analysis (CHN), displaying the suggested chemical composition of the produced Schiff base.[7] Yield: 87%, color white, FT. IR: 3194 cm^{-1}(OH of COOH), 1717 cm^{-1} (C=O St) 1618 cm^{-1} (-N=CH- St).^{1}H-NMR(500 MHz, DMSO- d_6(δ =13.3 ppm (4H COOH), 10 ppm (2H, -N=CH), δ = (8.86–8.20) ppm = (10 H, ArH). ^{13}C-NMR (500 MHz, DMSO-d_6: (166) ppm carbon atom of the carboxyl group and, (162) ppm, carbon of the

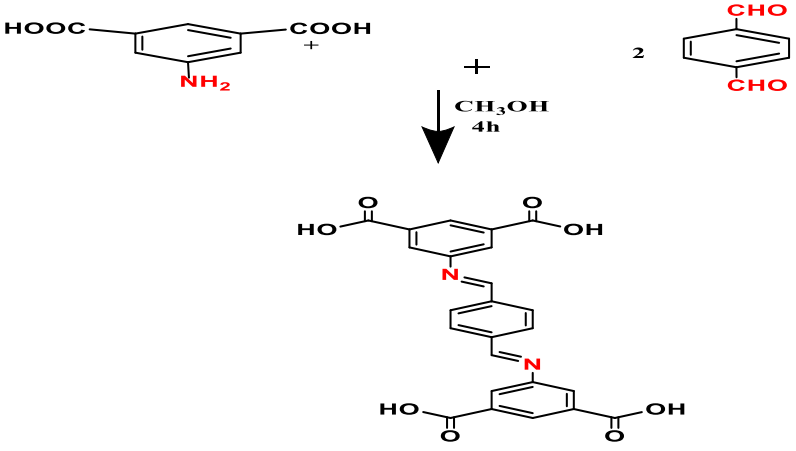

Fig. 1. Synthetic route of Schiff base compound [5A-T].

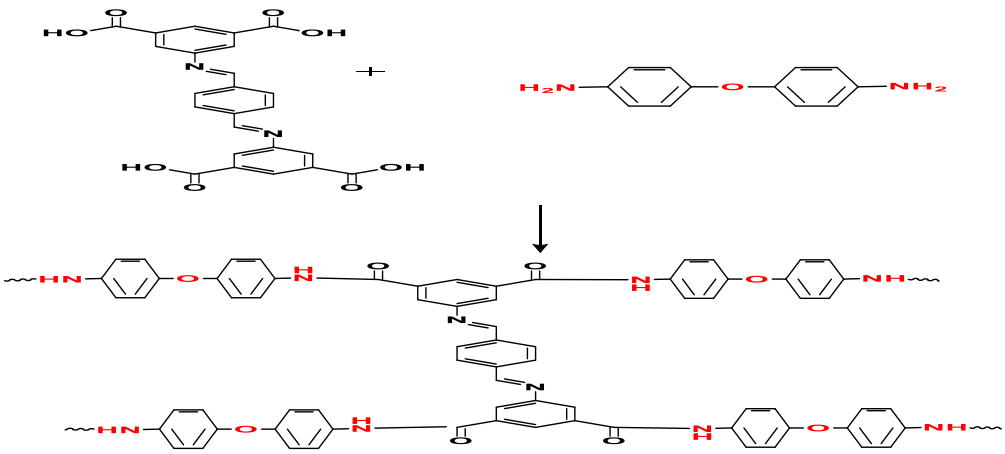

Fig. 2. Synthetic route of [P5A-T] chelate resin for [5A-T] Schiff base.

azomethine group (142) ppm and (117–138) ppm carbon atoms of the aromatic rings, in addition to the appearance of the signal of the carbon atoms of the DMSO solvent at (40) ppm.

Preparation of [P5A-T] chelates resin for [5A-T] Schiff base

The reaction apparatus is made up of a condenser, an addition orifice, a magnetic stirrer, and a circular, three-necked flask. Schiff base (5A-T), 4,4-oxydianiline (5mmol), 0.5g of lithium chloride, (3.1g, 10 mmol) triphenyl phosphite, 2.5 ml of pyridine, and 10 ml of N-methyl-2-pyrrolidone ((NMP)) were combined in a flask and heated to 100°C under nitrogen gas for 8–10 hours. A soft jelly was produced after the reaction was finished. The thick mixture was added to the cold methanol, and the resultant liquid was filtered and cleaned before being collected. The formula for chelated resin [P5A-T][8] is shown in Fig. 2. Additionally, using hot methanol to washed the resin and dried at 80°C. FT. IR: 3194 cm^{-1} (H-bonding), 1670 cm^{-1}, (C=O St amid), 1597cm^{-1} (-N=CH-).

Preparation of zinc iron oxide nanoparticles

The co-precipitation approach was used to create zinc iron oxide nanoparticles as a result of this process:

$$ZnCl_2 + 2FeCl_3 + 8NaOH \rightarrow ZnFe_4O_4 + 4H_2O + 8NaCl$$

First, two different zinc and iron chloride aqueous solutions were created: 3.6 g of $FeCl_3.6H_2O$ (13.3 mmol) and 0.9 g of $ZnCl_2$ (6.65 mmol) were dissolved in 40 ml of distilled water and stirred for 15 minutes. Second, the two solutions were added to a milliliter flask with a circular bottom and three necks. While waiting, a 0.5 M aqueous sodium hydroxide solution was prepared and slowly added while being violently mixed into the original solution. The addition took between 40 and 60 minutes to complete Depending on the necessary pH, a precipitation agent was added to the primary solution in amounts ranging from 80 to 100 ml. The pH readings taken at the end of each procedure therefore varied from 9 to 12. The reaction time was set at two hours, and the reaction temperature was set at 80°C. By bringing the created NPs to room temperature and repeatedly washing them in distilled water, the extra soluble salt was eliminated. After being placed in containers, the NPs powder was dried in an oven for 24 hours at 100 degrees Celsius.[9]

Preparation of magnetic zinc iron oxide composite resins

In a 500 ml flask with N_2, aromatic poly amide (0.6 g) was dissolved in 50 ml of N-methyl-2-pyrrolidone (NMP). Over the course of 60 minutes, the $ZnFe_2O_4$ nanoparticle/NMP suspension (50 ml) that was previously made was added drop by drop to the polymer solution. The suspension was put on a neodymium magnet to precipitate the magnetic particles after being stirred for 24 hours at room temperature. After that, in order to remove all polymers from the supernatant solution, NMP was employed to wash the magnetic particles. The particles were then dried in a vacuum oven at room temperature after a second methanol wash.[10]

Results and discussion

FTIR and ^{1}H-, ^{13}C-NMR analysis

A straightforward condensation procedure involving 2-to-1 mol ratios of 5-amino terephthalic acid and terephthaldehyde was used to create the tetra carboxylic acid monomer (5A-T).

A weak intensity stretch band was observed at the range (3194 cm^{-1}) due to aromatic CH vibration frequencies. The spectrum also recorded two strong stretching bands, the first in the range of 1717 cm^{-1} attributed to the bond (C=O) in the carboxyl group, while the second was in the frequency range (1618 cm^{-1}) belonging to the azomethine group. This came in agreement with what was mentioned in the literature, as the stretching frequency of the (C-N) bond appeared in the region (1313 cm^{-1}). In the corresponding resin, the emergence of a new wide band due to the reductive frequency of the NH group is noted. In addition, it is noted that the band of the carboxylic group belonging to the aromatic amine shifted to the lower frequencies cm^{-1} (1670 cm^{-1}), evidence of the formation of the amide bond. The azomethine group shifted to the lower frequencies in the cm^{-1} range (1597 cm^{-1}).

The ^{1}H-NMR spectra of this compound in a deuterium-substituted dimethyl sulfoxide solvent (DMSO-d_6) showed a single signal at (δH = 2.5) ppm, due to protons from traces of the solvent (DMSO) not deuterated. And a single signal at the site (δH = 3.3 ppm), due to the presence of traces of water, in this spectra. The H NMR spectrum of the monomer [5A-T] indicated in the appearance of a broad signal at ppm (δ =13.3ppm) due to the 4H carboxylic OH as well as the emergence of a signal due to the -N=CH- proton at δ = (10 ppm) and a multi-band signal due to aromatic ring protons at ppm (8.86–8.20 δ) is also visible in the spectrum. [11,12]

Table 1. Results of the elemental analyses and the average molecular weight calculations (Mw, Mn), polydispersity index (PDI), and ηinh.

%C	%H	%N	ηinh	(Mw)	(Mn)	PDI
62.61 (62.75)	3.50 (3.57)	6.08 (6.48)	0.85	38000	17000	2.2

^{13}C-NMR spectra were recorded for Schiff bases prepared using a solvent, dimethyl sulfoxide, as shown in the study with ^{13}C-NMR spectroscopy. We notice that the spectrum of the ligand (5A-T) consist of a signal at a chemical displacement (166) ppm that belongs to the carbon atom of the carboxyl group and a signal at ppm (162) ppm, belongs to the carbon of the azomethine group (142) ppm, and as the signals appeared, which fall within the ppm range (117–138), which belong to the carbon atoms of the aromatic rings, in addition to the appearance of the signal of the carbon atoms of the DMSO solvent at (40) ppm. [13,14]

Although the natural viscosity of the aramids could be increased by adding a suitable amount of LiCl to the reaction mixture, all polymerizations were therefore carried out in NMP containing lithium chloride. Polycondensation in NMP persisted evenly even in the absence of a metal salt that boosts the solubility of aramids, such as lithium chloride. Aramids with intrinsic viscosities of 0.8 dL/g were yielded practically quantitatively. For instance, aramids with intrinsic viscosities greater than 0.85 dL/g could be created by diamines with electron-donating ether groups in the para position. The aramids' molecular weight, determined by GPC and shown in Table 1, was determined. Mn and Mw values for the aramids were in the range of 17.000 and 38.000; respectively. The polydispersity index Mw/Mn. 2.2 is used to determine the molecular weight distribution. The molecular weight distribution of polymers produced by polycondensation is affected by the method of addition, the concentration of the monomers, the viscosity of the reaction fluid, and the regularity of stirring. In the present study, aramids with rather narrow molecular weight dispersion were synthesized. The TPP NMP/Py/LiCl mixture was used to create the azomethine polymers P5A-T, which have exceptional solubility in polar aprotic solvents like NMP, DMAc, DMF, DMSO, and even less polar solvents like pyridine and m-cresol. The high solubility should be caused by the presence of a number of functional groups in the polymer backbone, including ether linkage groups, amide joints, and an asymmetrical structure as shown in Table 2. These components made the P5A-T more soluble by promoting better solvent molecule penetration, the formation of

Table 2. Poly (Azomethine-amid) Solubility.

Solvent	Solubility	Solvent	Solubility
N, N-dimethylacetamide DMAc	+ +	Tetrahydrofuran	+
Dimethyl sulfoxide DSMO	+ +	Acetone	–
N-methyl-2-pyrrolidoneNMP	+ +	methanol	–
N,N´-di-methyl formamide DMF	+	m-Cresol-	–
Chloroform	+	Pyridine	+

Solubility: (+) soluble at room temperature, 'Partially soluble, and (–) insoluble.

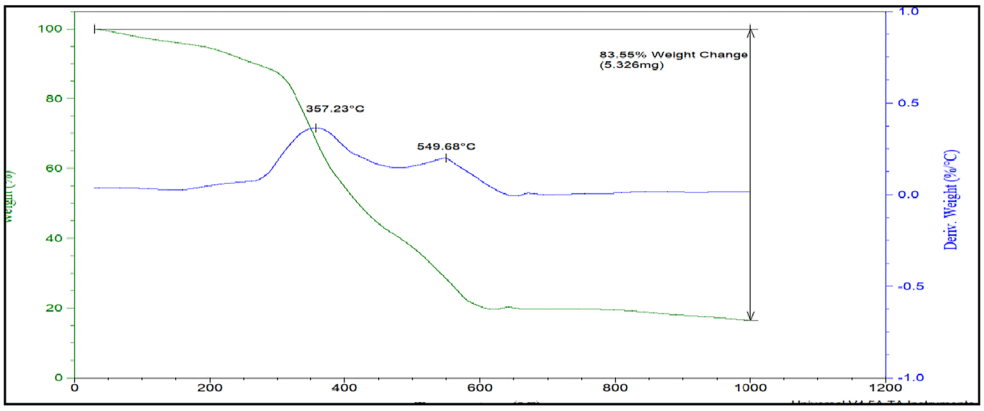

Fig. 3. Thermal analysis of the prepared P5A-T.

H-bonds, and dipole-dipole interactions with polar organic solvent molecules. The solubility also varies depending on the kind of dicarboxylic acid employed.

Thermal stability evaluations

The thermal stability of the polymer (P5A-T) was examined using TGA/DTG, and Fig. 3 depicts the weight loss curve. The thermo gravimetric analysis curves of the resin revealed the presence of two dissociation bands for the P5A-T resin, the first at 357.23°C and the second at 549°C. The findings indicated that the first stage is caused by the breakdown of amide groups, the second stage is brought on by the loss of functional aggregates containing the azomethine group, and the final stage is brought on by the thermal decomposition of the polymeric chains. [15]

Vibrating sample magnetometer (VSM)

Fig. 4a and Fig. 4b shows the variation of the magnetic field under an applied magnetic field at 300 K.

The synthesized sample is practically superparamagnetic, as seen by both images. The results show that pure $ZnFe_2O_4$ has a higher saturation magnetization value than P5A-T/$ZnFe_2O_4$. The MS value is influenced by a number of variables, including particle size, ion occupancy in the tetrahedral and octahedral positions, and cationic stoichiometry. Potential causes of the declining magnetization include the non-collinear magnetic structure; differences in super exchange interactions brought on by different coordination's, and spin canting. Because the polymeric covering successfully shielded the manganite, the polymer had a magnetic saturation value that is lower than what was anticipated for MNPs. However, due to their magnetic sensitivity and classification as superparamagnetic materials, these materials can quickly meet the demand for magnetic separation. [16,17]

Surface and elemental analysis

The shape of the zinc ferrite nanoparticles is shown in Fig. 5a. The $ZnFe_2O_4$ sample's SEM photos show irregularly shaped particles at various magnifications. Due to Fe ions, all the particles have formations that

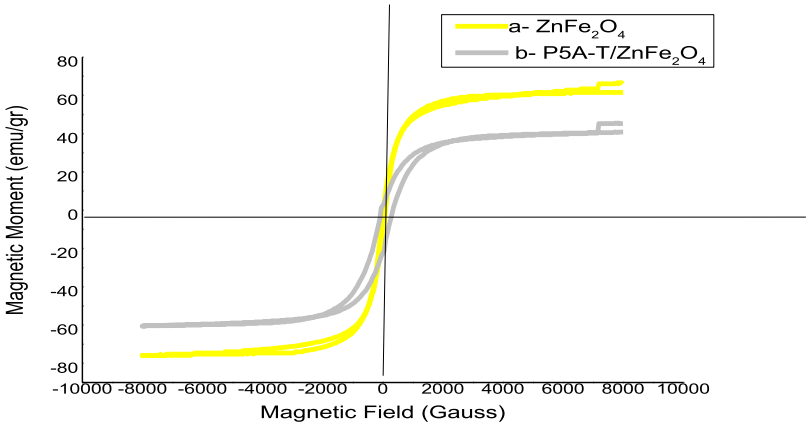

Fig. 4. Field dependence of magnetization for the $ZnFe_2O_4$ (a) and aromatic polyamide/$ZnFe_2O_4$ nanocomposite (b).

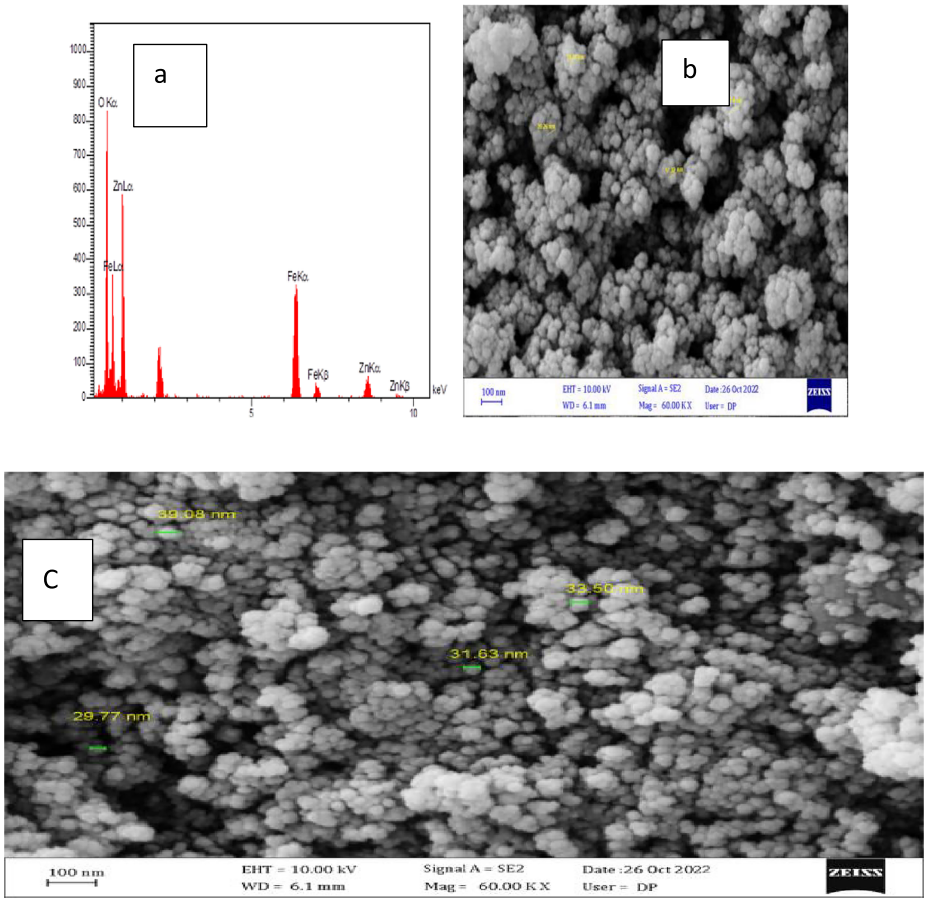

Fig. 5. FTSEM image of (a) $ZnFe_2O_4$, (b) EDX for $ZnFe_2O_4$, (c) P5A-T/$ZnFe_2O_4$.

resemble rocks. In a pure sample, no significant particle size was discovered. Due to aggregation and uneven shape, the surface morphology of all samples can be seen through SEM analysis in the rang (19–20 nm). The EDX pattern of a sample of synthesized $ZnFe_2O_4$ is shown in Fig. 5b. Table 3 below contains the elemental content of the samples I. The presence of chemical components including oxygen (O), zinc (Zn), and iron (Fe) elements was confirmed by EDX to be pure and formed.[18] As Fig. 5c, which depicts azomethine-amide composite resins with magnetic zinc iron oxide, demonstrates that they almost assumed the form of magnetic zinc iron oxide.

TEM images of Zn Fe_2O_4 NPs with average sizes of 7 nm and diameter ranges of 2 to 24 nm are shown in Fig. 6a and Fig. 6b displays Zn Fe_2O_4 NPs with a P5A-T coating on the core and particles as small as 36.5 nanometers. In Fig. 6b, P5A-T/Zn Fe_2O_4 NPs dispersion is depicted. The size distribution of the particles ranges from 30 to 80 nm, with the majority of them being less than 100 nm in size.[19,20]

Table 3. Elemental Analysis of $ZnFe_2O_4$.

Element	Weight%	Atomic%
O	31.41	62.82
Fe	43.02	24.65
Zn	57.25	12.52
Total	100.0	100.0

Nitrogen adsorption-desorption analysis

The specific surface area of P5A-T/$ZnFe_2O_4$ nanocomposites was calculated using BET. Fig. 7 and Table 4**.** display the N_2 adsorption-desorption isotherm and BJH pore size distribution map for P5A-T/$ZnFe_2O_4$ nanocomposites. The $ZnFe_2O_4$/P5A-T nanocomposite had an approximate average pore diameter of 39.01 nm, a specific surface area of 126.62 m^2g, and a total pore volume of 1.3455 cm^3g^{-1}.[21,22]

The zeta potential

A zeta analyzer was used to determine the suspension's zeta potential in the electrode cell Fig. 8. The

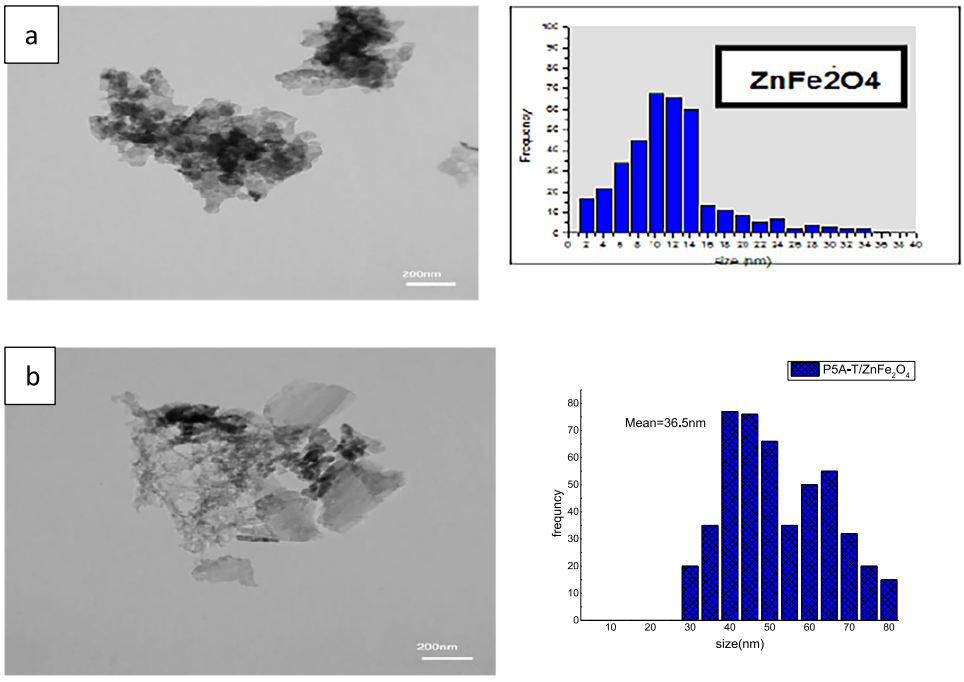

Fig. 6. (a) Zn Fe_2O_4 NPs and (b) P5A-T/Zn Fe_2O_4 Size Distribution Histograms from TEM.

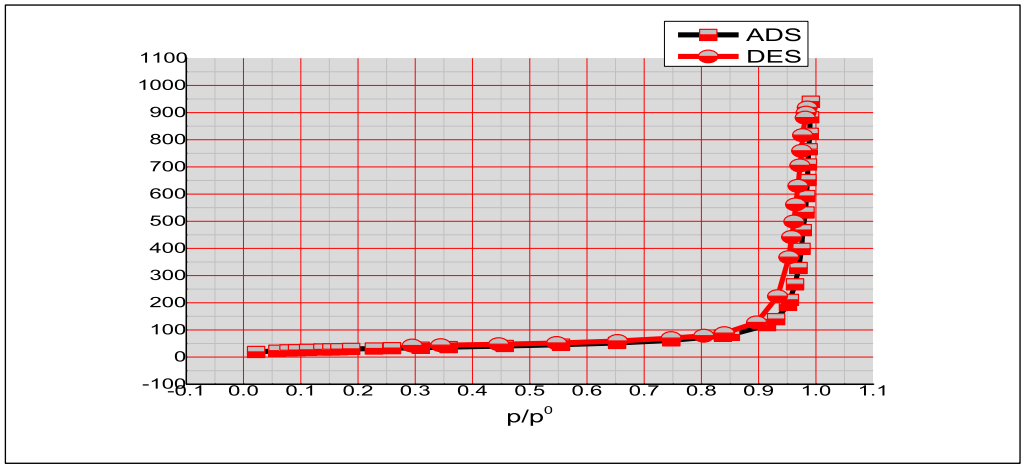

Fig. 7. Nitrogen adsorption-desorption.

P5A-T/$ZnFe_2O_4$ nanocomposite surface was found to have a negative charge for the whole range under investigation at the zeta potential (–39.9 mV). Given that P5A-T molecules are polar, the existence of an electric pull between them was theoretically supported by the nanocomposite polymer, which gave it stability and dependability.[23]

Table 4. Surface area and porosity information.

Property	P5A-A/Zn Fe_2O_4
Surface area (m^2/g)*	126.62
Pore volume (cm^3/g)**	1.3455
Pore diameter (nm)**	39.01
Isotherm type	mesopores

Measurements using dynamic light scattering (DLS) and transmission electron microscopy

Fig. 9 depicts Hydrodynamic radius values for magnetic zinc iron oxide particle sizes. Among the key elements in determining particle size are the particle size and hydrodynamic diameter. The size and form of the particles as well as the hydrodynamic radius were determined using TEM and dynamic light scattering (DLS). The hydrodynamic radius ranged from

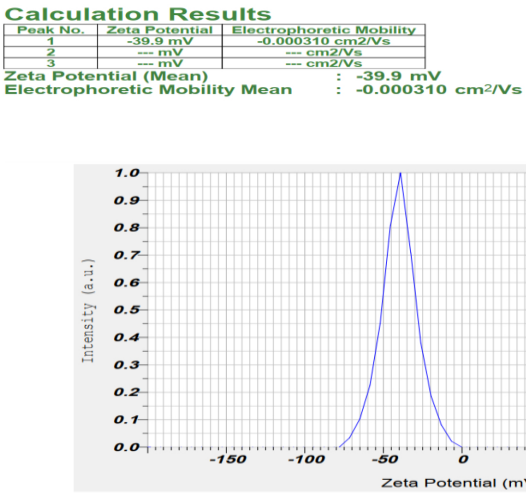

Fig. 8. The resin P5A-T/$ZnFe_2O_4$'s zeta potential values.

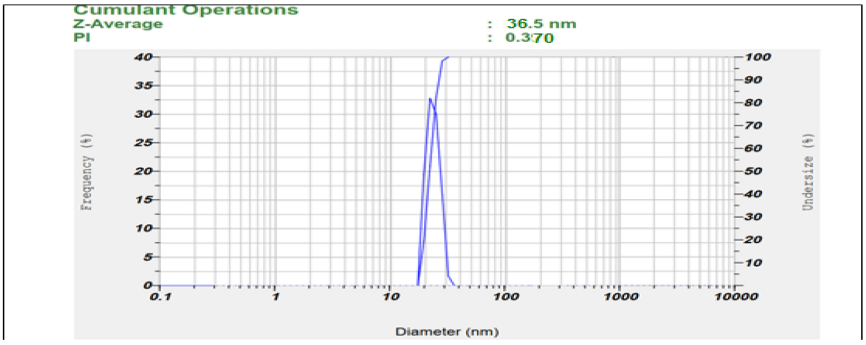

Fig. 9. Hydrodynamic radius values for magnetic zinc iron oxide particle sizes.

(36.5) nm whereas the zinc iron oxide nanoparticles were (19) nm in size. The multiple dispersion indexes, which measures dispersion was 0.37, indicating a monomorphic dispersion. The hydrodynamic diameter, in contrast to TEM, which measures particle size in the dry state, measures particle size in the liquid, where the particle is surrounded by various ionic layers of solvents attached in the solution because the particles in the solution have a random Brownian motion. The particle size was substantially bigger than that of what was detected by TEM due to the various interactions with solvent particles and other particles.[24,25]

X-ray diffraction (XRD) technology of $ZnFe_2O_4$

The diffraction pattern of X-rays (XRD) of $ZnFe_2O_4$ is shown in Fig. 10. Using X-ray diffraction tests carried out between 25° and 80°, the crystallite size and crystalline structure of the synthesized NPs were identified in Fig. 10. The diffraction characteristic peaks for this sample can be ascribed to the crystallographic planes (220), (311), (222), (400), (422), (511) and (440) at 2 θ equals to 29.89°, 35.21°, 36.84°, 42.79°, 53.08°, 56.58°, and 62.13°. The sample's diffraction patterns point to the presence of a special spinel cubic phase, matching the JCPDS card number 98-004-O456.[26]

Analytical study

Study of the analytical efficiency of the polymer (P5A-T/$ZnFe_2O_4$)

In this study, the Batch Method was used to study the analytical efficiency of the polymer [P5A-T/$ZnFe_2O_4$] towards a number of ions that were studied, which include, pb^{2+}, Cu^{2+} and Ni^{+2}, and the concentration of ions in these solutions was determined by flame atomic absorption spectroscopy. After shaking (10 ml) of the studied ion solution with a concentration of 100 ppm with 0.01 g of the polymer for 24 hours, the ions pb^{2+}, Cu^{2+} and Ni^{2+} showed a great response towards the polymer, so these ions have been studied in detail.

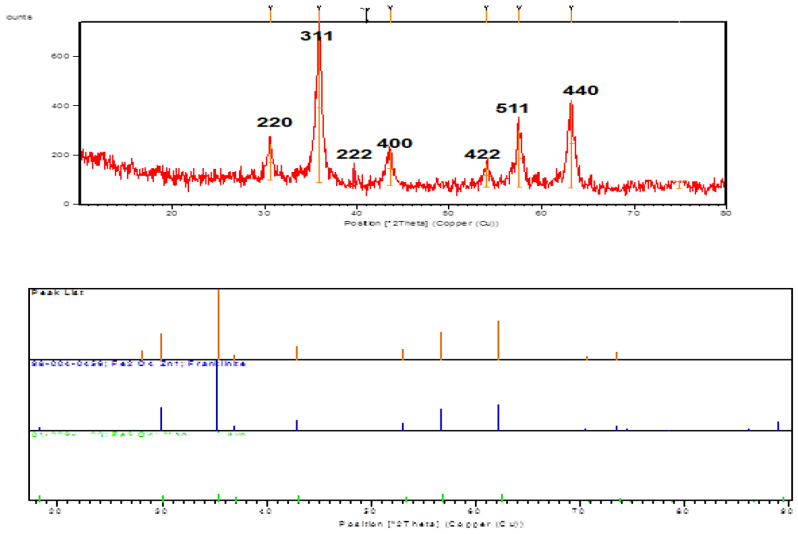

Fig. 10. X-ray diffraction spectrum of samples $ZnFe_2O_4$.

The effect of treatment time on the maximum loading capacity of the polymer (P5A-T/$ZnFe_2O_4$)

The effect of the treatment time was studied on the loading efficiency of the polymer [P5A-T/$ZnFe_2O_4$] in withdrawing ions of the studied elements, as it was observed that with increasing the treatment time of the studied ions solutions, the loading capacity of the polymer increased, the ions (Pb^{2+}, Cu^{2+}, Ni^{2+}) reach to the state of equilibrium after 0.5 hour has passed, and the amount of loading capacity increases slightly until 24 from the treatment reaching. Figs. 11 to 16 show the effect of treatment time on the polymer loading capacity [P5A-T/$ZnFe_2O_4$] for ions (pb^{2+}, Cu^{2+}, Ni^{2+}) in the studied pH functions.

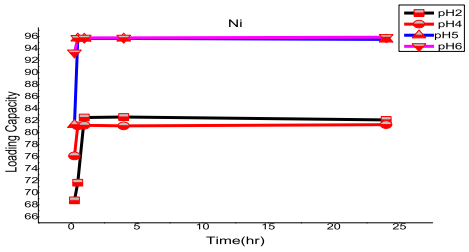

Fig. 11. The number of milligrams of Ni^{2+} withdrawn by (0.01g) of resin [P5A-T/$ZnFe_2O_4$] as a function of time at different pH levels.

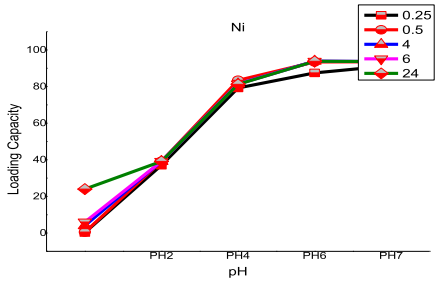

Fig. 12. The impact of the pH functions on the polymer's ability to load the lead ion at various treatment durations.

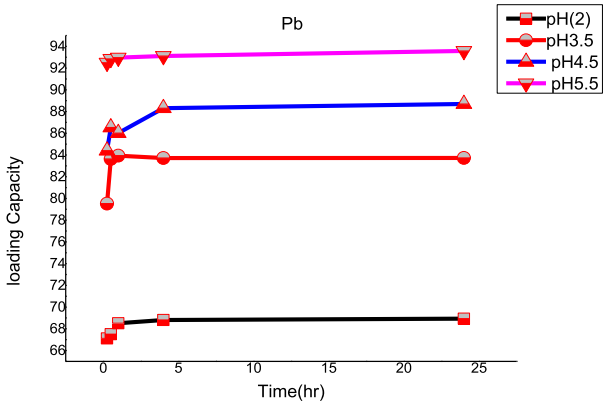

Fig. 13. The number of milligrams of Pb^{2+} withdrawn by (0.01g) of resin [P5A-T/$ZnFe_2O_4$] as a function of time at different pH levels.

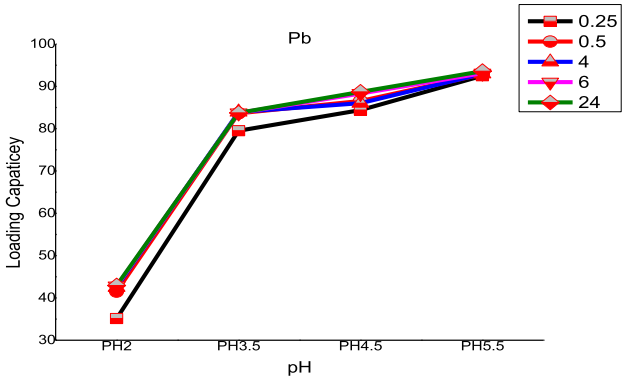

Fig. 14. The impact of the pH functions on the polymer's ability to load the lead ion at various treatment durations.

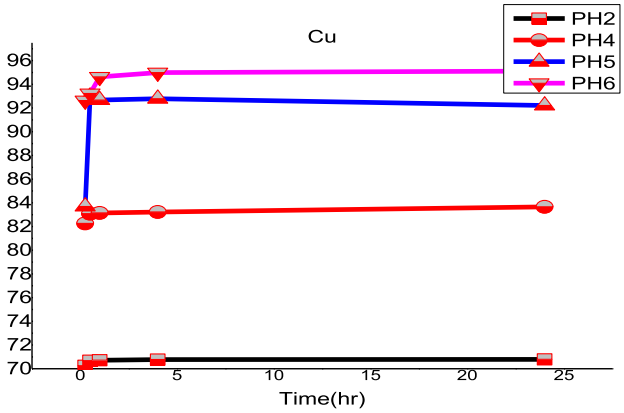

Fig. 15. The number of milligrams of Cu^{2+} withdrawn by (0.01g) of resin [P5A-T/$ZnFe_2O_4$] as a function of time at different pH levels.

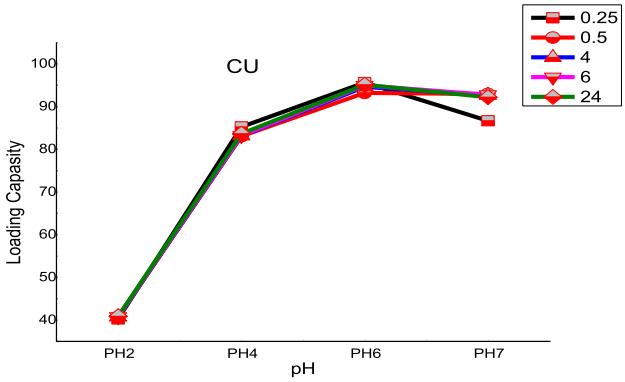

Fig. 16. The impact of the pH functions on the polymer's ability to load the lead ion at various treatment durations.

The effect of the pH function on the analytical efficiency of [P5A-T/$ZnFe_2O_4$] resins

The effect of the pH function on the loading efficiency of the polymer [P5A-T/$ZnFe_2O_4$] was studied in withdrawing the ions of the elements. The results obtained from the study of the acidity function indicate that the efficiency of the P5A-T/$ZnFe_2O_4$ resin towards the studied ions follows the following order $> Ni^{+2} > Pb^{+2} > Cu^{+2}$.

The pH is one of the crucial variables in the adsorption of metal ions onto chelated polymers, which is carried out by adsorbents in various acidic solutions. Depending on the pH level of the solution, the active functional groups that are present on the surface of the nano sorbent material might be protonated. It is evident for nonabsorbent resin that the values of adsorption capacity increase with increasing pH, though an increase in pH values above pH 7 can result in a potential precipitation of metal ions that inhibits the adsorption treatment. Then, at a low pH value, the adsorption capacity of heavy metal ions is relatively low, which may be explained by the competitive adsorption between the hydronium ion and the metal ions.

Moreover, the surfaces of the nano adsorbents appear to be positively charged due to the presence of a higher concentration of hydronium ion which reduces the number of binding sites for metal ions.[27] It was observed that the absorption of (Cu^{+2}, Ni^{+2}, Pb^{+2}) on the surface of the resin is low in acid solutions and with an increase in the pH values, where we find that the maximum absorption of ions at the pH value is approximately 6. A pH of less than 4 indicates that the active nitrogen atoms in the resin practically denaturant partially. In other words, at low pH values, H^+ ions compete with heavy metal ions for adsorption sites, as well as electrostatic repulsion between active protons and positively charged ions, and this limits the absorption capacity of the elements, and the opposite occurs in the case of the non-protonation of the nitrogen atom and the hydrolysis process leads to an increase in the adsorption of the elements. As for the adsorption mechanism, it should be noted that there are electron donor atoms such as oxygen in C=O and nitrogen in each of the amide and azomethine groups, and these can donate some of their electronic density in the Bay system (Bay succession) through resonance and there is an important effect due to the presence of the effect of Bay electrons Unsigned in the ligand, which affects the susceptibility of complexation (chelation) in the bonding structure, and we can say that the process of forming complexes takes place through oxygen atoms and nitrogen atoms in the azomethine group. The participation of physical forces like the Van der Waals forces with the chemical forces represented by the exchange of electrons and the formation of a chemical bond between metal ions and functional groups on the surface of the resin may be the cause of the high non-specific absorption of these ions. Effects of entropy, enthalpy, and other factors like ionic radius.

Competitive adsorption

Competitive adsorption was evaluated in a triple system consisting of three of the ions of the studied elements such as (pb^{2+}, Cu^{2+}, and Ni^{2+}) and in conditions after stabilizing the ideal conditions from time and acidity functions in a mixture of solutions. The results showed that the adsorption of element ions has decreased from the first adsorption. The reason for the lower rate of adsorption in the ternary system than in the monomeric system is the increase in the electrical repulsion between other metal cations in the solution that inhibit adsorption. It is possible that the obvious difference in the tendency of stronger bonding of Pb^{2+} and Cu^{2+} than Ni^{2+} is based on their ionic properties. such as ionic radius, acid-base solid theory, covalent indices, total binding strength

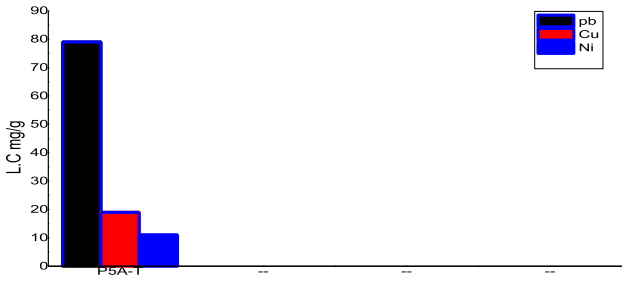

Fig. 17. Competitive adsorption of heavy metal ions in the ternary system.

Although Pb^{+2} and Cu^{+2} and Ni^{2+} have the same number of charges, Pb^{+2} and Cu^{+2} ions will be more strongly attracted to the surface of negatively charged resins due to higher crystal radius of (Pb^{2+} 1.20) and (Cu^{2+} 0.73) compared to (Ni^{2+} 0.69). In addition, the lower adsorption of Ni^{2+} ion may be related to its lower covalent index (4.99) compared to Pb^{2+} (6.6) and Cu^{2+} (6.32) and therefore Cu^{2+} and Pb^{2+} ions have a greater tendency than Ni^{2+} to form covalent bonds with the bond to the adsorbed surfaces. Pb^{2+} 1.94 and Cu^{2+} 2.22; therefore, Pb^{2+} and Cu^{2+} show greater access to a particular pore surface than other ions, which leads to a higher degree of adsorption, Fig. 17 illustrates this.[28–31]

Regeneration of the loaded polymers

The regeneration of the resins and the recovery of chelated metal ions was carried out as following: The loaded resin was treated with HCl solution of a predetermined normality (1N) and volume (the same volume of treatment time study from 0.25 hrs. to 24 hrs. after which the solution was filtered and the concentration of the studied ions was determined by (F.A.A.) from calibration curves prepared with(1N) HCl at the same eluent concentration, percentage ion recovery for each ion was plotted as a function of time. Fig. 18 illustrates this.

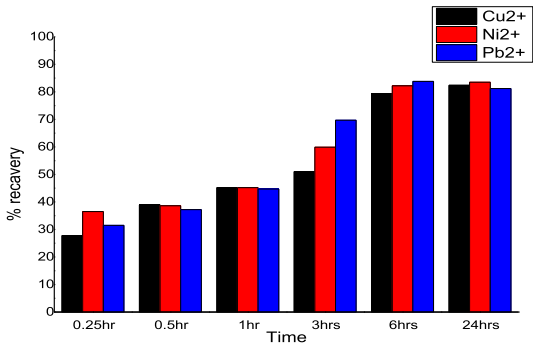

Fig. 18. The effect of treatment time on uptake ions of polymer.

Conclusion

A novel azomethine tetra carboxylic acid monomer with good thermal stability was successfully used to create magnetic ladder-type poly (azomethine amide). Spectroscopic techniques verified the molecular structures of the monomers and the resulting polymers. The polymers in this work had reasonably good yields, high Mw, and ηinh thanks to a relatively straightforward polymerization process. Afterwards, it was discovered that these polyamides had a good balance between the properties (thermal stability versus solubility). High magnetism was exhibited by $ZnFe_2O_4$ and P5A-T/$ZnFe_2O_4$, which was readily and rapidly separated from aqueous solution by an external magnetic field. The polyamides were resistant to chemicals and may be used to remove heavy metal ions from industrial waste as much as 95 mg/g of polymer and the polymer retains its sorption behaviors and has a high regeneration ability of up to 95%. Polymers have a very high loading capacity for Ni^{2+}, Pb^{2+} and Cu^{2+}. The polymers' highly effective competitive adsorption and ability reuse toward Pb (II), Ni(II), Cu(II).

Acknowledgement

The author would like to express deep appreciation to the Department of Chemistry at the College of Education for Pure Science at University of Basrah / Iraq for their assistance in the lab work and analysis.

Authors' declaration

- Conflicts of Interest: None
- I hereby confirm that all the Figures and Tables in the manuscript are mine. Any Figures and images, that are not mine, have been included with the necessary permission for re-publication, which is attached to the manuscript.
- No animal studies are present in the manuscript.
- No human studies are present in the manuscript.
- Ethical Clearance: The project was approved by the local ethical committee at General Directorate of Basra Education.

References

1. Shui L, Pan X, Chen X, Chang F, Wan D, Liu D, *et al.* Pollution characteristics and ecological risk assessment of heavy metals in sediments of the three gorges reservoir. Water. 2020;12(6):1798. https://doi.org/10.3390/w12061798.
2. Reham H, Nehad A, Manal M, Amal HA. Adsorption of Ni(II) and Fe(II) Ions Using Cross- Linked Modified Chitosan-

Khellinone Schiff's Base for Waste Water Treatment: Int J Innov Res Sci Eng Technol. June 2015;4(6):2319–8753 https://doi.org/10.15680/IJIRSET.2015.0406144.
3. Al Dabbagh BM, Kadhim HJ, Salih RM. Studying the effect of Polyamide 6 Nanofibers on Physical and Chemical Properties of Unsaturated Polyester Reinforced by Glass Fibers Composites. IOP Conf Ser: Mater Sci Eng. Nov 2020;757(012001):1–6. https://doi.org/10.1088/1757-899X/757/1/012001.
4. Myrovali E.- PhD thesis Magnetic Nanoparticle Arrays: Features, Properties, Applications, Aristotle University of Thessaloniki, 2020, Greece, Ag. Dimitriou, Thessaloniki.
5. Hakeem HS, Abbas NK. Preparing and studying structural and optical properties of Pb1-xCdxS nanoparticles of solar cells applications. Baghdad Sci J. 2021;18(3):640–648. http://dx.doi.org/10.21123/bsj.2021.18.3.0640.
6. Moises BT, David RF, Belén A V, Samantha P, Emilio B. Interaction between Filler and Polymeric Matrix in Nanocomposites: Magnetic Approach and Applications, Polymeres (Basel). Sep 2021;13(17):2998. https://doi.org/10.3390/polym13172998.
7. Murugesan A, Ravikumar L, SathyaSelvaBala V, SenthilKumar P, Vidhyadevi T, Dinesh Kirupha S, *et al.* Removal of Pb(II), Cu(II) and Cd(II) ions from aqueous solution using polyazomethineamides: Equilibrium and kinetic approach. 2011;271(1–3):199–208. https://doi.org/10.1016/j.desal.2010.12.029.
8. José A, Reglero RI, Miriam TL, Félix CG, José MG. Functional Aromatic Polyamides. Polymers. Sep 2017;9(12):414. https://doi.org/10.3390/polym9090414.
9. Panda SK, Aggarwal I, Kumar H, Prasad L, Kumar A, Sharma A, *et al.* Magnetite nanoparticles as sorbents for dye removal: A review. Environ Chem Lett. Jun 2021;19(3):2487–2525. https://doi.org/10.1007/s10311-020-01173-9
10. Wei S, Zhu Y, Zhang Y, Xu J. Preparation and characterization of hyper branched aromatic polyamides/Fe_3O_4 magnetic nanocomposite. React Funct Polym. 2006;66(11):1272–1277. https://doi.org/10.1016/j.reactfunctpolym.2006.03.008.
11. Zeydi MM, Kalantarian SJ, Kazeminejad Z. Overview on developed synthesis procedures of coumarin heterocycles. J Iran Chem Soc. 2020;17:3031–3094. http://dx.doi.org/10.1007/s13738-020-01984-1.
12. Abbas GJ, Mosaa Z, Radhi AJ, Abbas HK, Najem WM. Synthesis, studying analytical properties and biological activity of new transition metal complexes with sulfadiazine derivative as reagent. Egypt J Chem. 2023;66(1):55–61. https://doi.org/10.21608/EJCHEM.2022.104212.4814.
13. Omdi S, Khojasteh V, Kakonejadfard A, Ghasemion M, Azarbani F. Synthesis, characterization, spectroscopy and biological activity of 4-(3-formyl-4-hydroxyphenyl azol)-1-alkylpyridinium salts, J Chem Sci. Aug 2018;130:114. https://doi.org/10.1007/s12039-018-1521-5.
14. Osman UM, Silvarajoo S, Kamarudin KH, Tahir MIM, Kwong HC. Ni_2+ complex containing a thiosimicarbazone ligand: synthesis, spectroscopy, single crystal x-ray crystallographic and conductivity studies. J Mol Struct. 2021;1223:128992. https://doi.org/10.1016/j.molstruc.2020.128994.
15. Hajibeygi M, Fardi M, Shabanian M. New nanocomposites based on polyamide containing imine groups reinforced with functionalized polyethyleneimine-modified ZnO nanoparticles; fabrication, characterization and lead ion adsorption studies. Polym Composite. July 2019;40(7):2602–2616. https://doi.org/10.1002/pc.25055.
16. Pengfei Y, Yaping Y, Mingwen W. Catalytic ozonation of phenol by $ZnFe_2O_4$/ZnNCN: performance and mechanism, Environ Sci Pollut Res Int. Dec 2022;29(58):88172–88181. https://doi.org/10.1007/s11356-022-21696-8.
17. Sung YH, Ye CK, Mei W, Jae DN, Jonghwan S. Synthesis of Fe_3O_4 composite particles by emulsion polymerization. IOP Conf Ser Earth Environ Sci. July 2020;565:012050 IOP Publishing. https://doi.org/10.1088/1755-1315/565/1/012050.
18. Kareem SH, Naji AM, Taqi ZJ, Jabir MS. Polyvinylpyrrolidone Loaded $MnZnFe_2O_4$ Magnetic nanocomposites Induce Apoptosis in Cancer Cells Through Mitochondrial Damage and P 53 Pathway. J Inorg Organomet Polym Mater. July 2020;30(1–2):5009–5023 https://doi.org/10.1007/s10904-020-01651-1.
19. Jassim RA, Farhan AM, Ali AM. Corrosion protection study of carbon steel and 316 stainless steel alloys coated by nanoparticles. Baghdad Sci J. 2014;11(1):116–122. https://doi.org/10.21123/bsj.2014.11.1.116-122.
20. Hammadi AH, Jasim AM, Abdulrazzak FH, Al-Sammarraie A, Cherifi Y, Boukherroub R, *et al.* Purification for carbon nanotubes synthesized by flame fragments deposition via hydrogen peroxide and acetone. Materials. May 2020;13(10):2342. https://doi.org/10.3390/ma13102342.
21. Musa A, Wada Bawa H, Mohammed AH, Mohammed AD. Green Synthesis of Silver Nanoparticles and Its Antibacterial Activity using the Flower Extract of Senna Siamea. Int J Nanosci Nanotechnol. 2021;17(3):173–179.
22. Patel AR, Sereda G, Banerjee S. Synthesis, characterization and applications of spinel cobaltite nanomaterials. Curr Pharm Biotechnol. May 1 2021;22(6):773–92. https://doi.org/10.2174/1389201021666201117122002.
23. Kavinkumar T, Vinodgopal K, Neppolian B. Development of nanohybrids based on porous spinel MCO_2O_4 (M = Zn, Cu, Ni and Mn)/reduced graphene oxide/carbon nanotube as promising electrodes for high performance energy storage devices. Appl Surf Sci. May 30 2020;513:145781. https://doi.org/10.1016/j.apsusc.2020.145781.
24. Souza TG, Ciminelli V, Mohallem NDS. A comparison of TEM and DLS methods to characterize size distribution of ceramic nanoparticles. J Phys Conf Ser. July 2016;733(1):012039. https://doi.org/10.1088/1742-6596/733/1/012039.
25. Christopher MH, Natasha S, Paul W, Martha LM. A comparison of atomic force microscopy (AFM) and dynamic light scattering (DLS) methods to characterize nanoparticle size distributions. J Nanopart Res. June 2008;10,89–96. https://doi.org/10.1007/s11051-008-9435-7.
26. Ait Kerroum MA, Essyed A, Iacovita C, Baaziz W, Ihiawakrim D, Mounkachi O, *et al.* The effect of basic pH on the elaboration of $ZnFe_2O_4$ nanoparticles by co-precipitation method: structural, magnetic and hyperthermia characterization. J Magn Magn Mater. May 2019;478(15):239–246. https://doi.org/10.1016/j.jmmm.2019.01.081.
27. Botelho Junior AB, Dreisinger DB, Espinosa DCR. A Review of Nickel, Copper, and Cobalt Recovery by Chelating Ion Exchange Resins from Mining Processes and Mining Tailings. Min Metall Explore. Nov 2019;36:199–213 https://doi.org/10.1007/s42461-018-0016-8.
28. Salehi N, Moghimi A, Shahbazi, H. Preparation of cross-linked magnetic chitosan with methionine-glutaraldehyde for removal of heavy metals from aqueous solutions. Int J Environ Anal Chem. 2020;102(10):1–17. https://doi.org/10.1080/03067319.2020.1753718.
29. Kareem MM, Kadem BY, Mohammad EJ, Atiyah AJ. Synthesis, Characterization and Gas Sensor Application of New Composite Based on MWCNTs: CoPc: Metal Oxide. Baghdad Sci J.

2021;18(2):384–392. https://dx.doi.org/10.21123/bsj.2021.18.2.0384.

30. Deng J, Liu Y, Liu S, Zeng G, Tan X, Huang B, *et al.* Competitive adsorption of Pb(II), Cd(II) and Cu(II) onto chitosan-pyromellitic dianhydride modified biochar. J Colloid Interface Sci. July 2017;506:355–364. https://doi.org/10.1016/j.jcis.2017.07.069.

31. Shaalan N, Mahdi S. Synthesis, Characterization and Biological activity Study of Some New Metal Complexes With Schiff's Bases Derived from [*O*-Vanillin] With [2-Amino-5-(2-Hydroxy-Phenyl)-1,3,4-Thiadiazole]. Egypt J Chem. 2021;64(8):4059–4067. https://dx.doi.org/10.21608/ejchem.2021.66235.3432.

امتزاز الرصاص(II) ، والنحاس(II) ، والنيكل (II) بواسطة راتنج لقاعدة شيف المغناطيسية الجديدة: التحضير والتشخيص ودراسة حرارية

ايمان سعد علي

المديرية العامة لتربية البصرة، البصرة، العراق.

الخلاصة

تناولت هذه الدراسة تحضير ودراسة تحليلية لنوع من الراتنجات المخلبية ، تميز هذا النوع من الراتنجات باحتوائه على ليكاند من نوع قواعد شف الاروماتية (5A-T) والذي انتجه تفاعل الامين الاروماتي(5-aminoisopthalic acid) مع الترفثالديهايد وقد شخصت قاعدة شف المحضرة باستخدام تقنية مطيافية الاشعة تحت الحمراء FT- IR ومطيافية الرنين النووي المغناطيسي ^{1}H-NMR, ^{13}C-NMRو تقنية تحليل العناصر الدقيق. قواعد شف المحضرة تم تحويلها الى راتنج ازوميثين- امايد P5A-T وذلك بمفاعلة الليكاند (5A-T) مع الامين الثنائي (4,4-oxydianiline) وقد شخص الراتنج المحضر باستخدام تقنية مطيافية الاشعة تحت الحمراء.

كذلك تضمنت الدراسة تحضير اوكسيد الحديد الخارصين المغناطيسي $ZnFe_2O_4$ بطريقة الترسيب التساهمي وتطعيمه بالراتنج المحضر P5A-T وقد جرى تشخيص اوكسيد الحديد الخارصين المغناطيسي والراتنج المركب بعدة تقنيات منها المجهر الالكتروني الماسح FE-SEM اذ بينت الدراسة ان حجم الجسيمات (22nm) لأوكسيد الحديد الخارصين و (36 nm) للراتنج المغناطيسي المركب، علاوة على ذلك استخدمت تقنية حيود الاشعة السينية XRD في عملية التشخيص واكدت النتائج صحة التركيب المحضر، وفضلا عن ذلك درست الخواص المغناطيسية لأوكسيد الحديد الخارصين و الراتنج المحضر واظهرت للراتنج المركب سلوك مغناطيسي فائق واستخدم جهاز Malven Zetasizer لقياس جهد زيتا بتقنية DLS كما درست مساحة السطح باستخدام ايزوثيرم BET. الجزء الاخير تضمن دراسة الكفاءة التحليلية في امتزاز بعض ايونات العناصر الثقيلة (Ni^{+2}, Pb^{+2} , Cu^{+2}) باستخدام طريقة الوجبة Batch Method وباستخدام مطيافية الامتصاص الذري اللهبي وقد درست سعة التحميل للراتنجات المحضرة عند مختلف الظروف مثل الدالة الحامضية وزمن المعاملة, وكان ترتيب الانتقائية Pb(II) > Cu(II) > Ni(II).

الكلمات المفتاحية: مادة مازة، راتنج مخلبي، مغناطيسي، جسيمات نانوية، بولي ازوميثين.